SUPPLEMENTAL MATERIAL

Evidence of an improper displacive phase transition in $Cd_2Re_2O_7$ via time-resolved coherent phonon spectroscopy

J. W. Harter,[1,2] D. M. Kennes,[3] H. Chu,[2,4] A. de la Torre,[1,2] Z. Y. Zhao,[5,6]
J.-Q. Yan,[5,7] D. G. Mandrus,[5,7] A. J. Millis,[3,8] and D. Hsieh[1,2]

[1]*Department of Physics, California Institute of Technology, Pasadena, CA 91125, USA*
[2]*Institute for Quantum Information and Matter, California Institute of Technology, Pasadena, CA 91125, USA*
[3]*Department of Physics, Columbia University, New York, NY 10027, USA*
[4]*Department of Applied Physics, California Institute of Technology, Pasadena, CA 91125, USA*
[5]*Materials Science and Technology Division, Oak Ridge National Laboratory, Oak Ridge, TN 37831, USA*
[6]*Department of Physics and Astronomy, University of Tennessee, Knoxville, TN 37996, USA*
[7]*Department of Materials Science and Engineering, University of Tennessee, Knoxville, TN 37996, USA*
[8]*Center for Computational Quantum Physics, The Flatiron Institute, New York, NY 10010, USA*

S1. METHODS SUMMARY

Sample growth and characterization. Single crystals of $Cd_2Re_2O_7$ were grown by vapor transport[S1]. X-ray diffraction measurements were performed on pulverized single crystals using a PANalytical X'Pert Pro powder x-ray diffractometer with Cu $K\alpha_1$ radiation. No impurity peaks were observed. An elemental analysis was performed using a Hitachi TM-3000 scanning electron microscope equipped with a Bruker QUANTAX 70 energy dispersive x-ray system. The analysis confirmed an equal amount of Cd and Re within the resolution of the instrument. Magnetic susceptibility measurements were performed using a Quantum Design Magnetic Property Measurement System at temperatures from 2 to 350 K. The results indicated high quality crystals without the presence of ReO_2 inclusions.

Time-resolved reflectivity measurements. Pump-probe linear reflectivity experiments were performed using a regeneratively amplified Ti:sapphire laser system operating at a 10 kHz repetition rate with a center wavelength of 795 nm and a pulse duration of 80 fs. Pump and probe beams were cross polarized and focused onto the (111) surface of a $Cd_2Re_2O_7$ single crystal at near-normal incidence. The relative change in reflectivity of the probe beam was measured with a lock-in amplifier referenced to the pump beam mechanically chopped at 5 kHz. For pump fluences between $\sim$0.5 mJ/cm^2 and $\sim$3 mJ/cm^2, the reflectivity transients were found to scale linearly with fluence. Data shown in Fig. 2 of the main text were acquired with a pump fluence of 1.4 mJ/cm^2, well within the linear response regime, and a probe fluence of less than 100 μJ/cm^2.

Time-resolved SHG measurements. Pump-probe SHG experiments were performed using a regeneratively amplified Ti:sapphire laser system operating at a 100 kHz repetition rate with a center wavelength of 800 nm and a pulse duration of 100 fs. An optical parametric amplifier was used to convert the pump beam wavelength to 1400 nm. The obliquely incident 800 nm probe beam was S-polarized [parallel to the (111) surface] with a fluence of 600 μJ/cm^2 and the P-polarized response of the reflected SHG at 400 nm was measured with an electron-multiplying charge-coupled device camera. The scattering plane was oriented at the angle of maximum SHG intensity. Further details of the nonlinear optical setup can be found in Ref. S2.

Time-dependent Landau theory. Here we sketch a calculation of the damping of a

secondary phonon mode due to its coupling to primary critical modes. Further details can be found in Section S4. We make the assumption that a linearized theory applies (we are sufficiently far from T_c that true critical fluctuations are irrelevant), and that the primary modes have simple overdamped dynamics. The key point is that in the ordered phase, there is a linear coupling between fluctuations of the primary and secondary order parameters which leads to a damping of the secondary mode by the critical slowing down of the primary mode. In addition, because we have a linear coupling between the two modes, momentum is conserved and we need only consider the $k = 0$ excitations. A nonlinear coupling of the mode fluctuations would induce additional effects.

We start from Eqn. (4) of the main text and simplify the notation by rescaling $\Psi_{u,g}$ so that $a = 1$, rescaling Φ so that $b = 1$, and defining $u = c/a^2$ and $\bar{g} = g/a\sqrt{b}$. Dropping the constant term, defining $t = 1 - T/T_c$, and rearranging, we obtain

$$F = \frac{1}{2}\left(\Phi - \bar{g}\Psi_g\Psi_u\right)^2 - \frac{t}{2}\left(\Psi_u^2 + \Psi_g^2\right) + \frac{u}{4}\left(\frac{1-\lambda}{2}\left(\Psi_g^2 + \Psi_u^2\right)^2 + \frac{1+\lambda}{2}\left(\Psi_g^2 - \Psi_u^2\right)^2\right), \quad \text{(S1)}$$

with $\lambda = \bar{g}^2/u = g^2/bc \geq 0$. Here, $|\lambda| < 1$ is required for stability. This equation is minimized when $\Psi_u^2 = \Psi_g^2 = \bar{\Psi}^2/2$ and $\Phi = \bar{\Phi}$, with

$$\bar{\Psi}^2 = \frac{2t}{u\left(1-\lambda\right)} \qquad \bar{\Phi} = \frac{\bar{g}t}{u\left(1-\lambda\right)}. \quad \text{(S2)}$$

[Note: our assumption that Ψ_u and Ψ_g appear symmetrically in the free energy makes the analytical calculations much simpler. But the main results will not change even if this symmetry is not assumed].

We now expand the free energy around these equilibrium values, finding

$$\delta F = \frac{1}{2}\begin{pmatrix} \delta\Phi & \delta\Psi_+ & \delta\Psi_- \end{pmatrix} \mathbf{K} \begin{pmatrix} \delta\Phi \\ \delta\Psi_+ \\ \delta\Psi_- \end{pmatrix}, \quad \text{(S3)}$$

with $\delta\Psi_\pm = \left(\delta\Psi_u \pm \delta\Psi_g\right)/\sqrt{2}$ and force constant matrix $\mathbf{K}$ given by

$$\mathbf{K} = \begin{pmatrix} 1 & -\bar{g}\bar{\Psi} & 0 \\ -\bar{g}\bar{\Psi} & -t + \frac{3}{2}u\bar{\Psi}^2 - \bar{g}\bar{\Phi} & 0 \\ 0 & 0 & -t + \frac{3}{2}u\bar{\Psi}^2 + \bar{g}\bar{\Phi} \end{pmatrix}. \quad \text{(S4)}$$

We see that $\delta\Psi_-$ decouples. Assuming oscillating dynamics for the Φ mode (our units imply the dynamical term is ω^2/ω_0^2, with ω_0 the bare oscillation frequency of the Φ mode) and

overdamped dynamics for the Ψ modes (bare relaxation rate γ_0), we find that the dynamical matrix giving the response of the coupled modes is

$$\mathbf{D}(\omega) = \left[\begin{pmatrix} \frac{\omega^2}{\omega_0^2} - 1 & \bar{g}\bar{\Psi} \\ \bar{g}\bar{\Psi} & i\frac{\omega\gamma_0}{\omega_0^2} + t - \frac{3}{2}u\bar{\Psi}^2 + \bar{g}\bar{\Phi} \end{pmatrix} \right]^{-1}. \tag{S5}$$

The overdamped dynamics of the Ψ mode is nontrivial. If the mode is a long wavelength electronic fluctuation, the damping of the $k = 0$ component would vanish in a clean system. We expect that the real damping will be sample-dependent and involve the sample mean free path as well as spin-orbit coupling.

The experimental response is proportional to the Fourier transform of the $\delta\Phi$-$\delta\Phi$ component of the dynamical matrix. The result can be written in terms of the frequency $\Omega_0 = \omega_0\sqrt{1-\lambda}$ as

$$\mathbf{D}_{11}(\omega) = \frac{\frac{\Omega_0^2}{1-\lambda}}{\omega^2 - \Omega_0^2 - \Pi(\omega)}, \tag{S6}$$

with mode self-energy

$$\Pi(\omega) = \Omega_0^2 \frac{\lambda}{1-\lambda} \frac{-i\frac{\omega\Gamma}{\Omega_0^2} + \left(\frac{\omega\Gamma}{\Omega_0^2}\right)^2}{1 + \left(\frac{\omega\Gamma}{\Omega_0^2}\right)^2} \tag{S7}$$

where the effective relaxation rate

$$\Gamma = \frac{(1-\lambda)^2}{2t}\gamma_0 \tag{S8}$$

diverges as $T \to T_c$. We are interested in the case where $\gamma_0(1-\lambda)^2 \ll \Omega_0$. For $T \ll T_c$ ($t \sim 1$), the mode self energy Π is small and Ω_0 is the observed mode frequency. As t increases towards T_c, the mode broadening (inverse lifetime) $\lambda\Gamma/(1-\lambda)\Omega_0$ becomes appreciable and proportional to $1/t$ (see Fig. 4 of the main text). For the lifetime of the mode, we thus obtain $\tau \propto t = 1 - T/T_c$, in accordance with the experiment. As t is further decreased, the real part of Π starts to become important and the mode frequency shifts up. The experimental data, which indicate a weak effect on the frequency but a large effect on the damping, thus favor a scenario where $\lambda/(1-\lambda)$ is relatively large and $\Gamma < \Omega_0$.

S2. REFLECTIVITY TRANSIENTS CLOSE TO T_c

Time-resolved reflectivity transients were also acquired from $Cd_2Re_2O_7$ in the temperature window 180 K $< T \leq$ 200 K. However in this temperature window the lifetime of

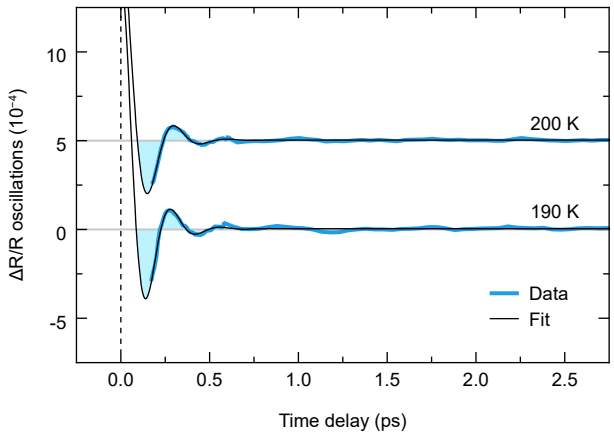

FIG. S1: **Time-resolved optical reflectivity.** Oscillations in $\Delta R/R$ after removal of an exponential background at $T = 190$ K and $T = 200$ K. Curves are vertically offset for clarity. Fits to the data were performed using the same procedure as that used in Fig. 2 of the main text.

mode 1 becomes so short that it is impossible to reliably extract the mode parameters by fitting the data. As shown in Fig. S1, the data at $T = 190$ K and $T = 200$ K look nearly indistinguishable from the data above T_c (see Fig. 2 of main text) and do not exhibit a clear presence of mode 1. Therefore no fit parameters for mode 1 are plotted above $T = 180$ K in Fig. 3 of the main text. Note that the lifetime τ we report is the $1/e$ value. Therefore even though τ_1 is less than one period of mode 1 just below 180 K, mode 1 is still detectable for some time beyond τ_1 and so, in practice, we fit to more than one period.

S3. ANALYSIS OF RAMAN DATA

In this section, we re-analyze the Raman spectroscopy data of Ref. S3. In particular, we fit the data shown in their Fig. 2(b) using a model of an underdamped harmonic oscillator identical to that discussed in the main text. Such an analysis is well-established in the Raman literature[S4,S5]. Fig. S2a shows the Raman data for a selection of temperatures, as well as fits to the equation

$$I_{\mathrm{Raman}}(\omega) = A + B\frac{(\omega_0/\tau)^2}{(\omega_0^2 - \omega^2)^2 + 4(\omega/\tau)^2}, \tag{S9}$$

where A and B are extrinsic constants capturing background and signal intensity, respectively, τ is the oscillator lifetime (inverse damping constant), and ω_0 is the natural frequency

of the oscillator. This equation represents the response of a damped harmonic oscillator $[\ddot{x} + (2/\tau)\dot{x} + \omega_0^2 x = 0]$ to a periodic drive at frequency ω and has been used to describe Raman spectroscopy of underdamped phonon modes[S4,S5]. Most notably, the resulting peak position of the equation is $\omega_{\text{peak}} = \sqrt{\omega_0^2 - 2/\tau^2}$, which can deviate significantly from ω_0, especially when τ is small. Reinterpreting the Raman data using this analysis, we see that the data is consistent with a weak temperature dependence of the oscillator natural frequency (Fig. S2b) and a strong temperature dependence of the oscillator lifetime (Fig. S2c), which grows from near zero at T_c, as discussed in the main text.

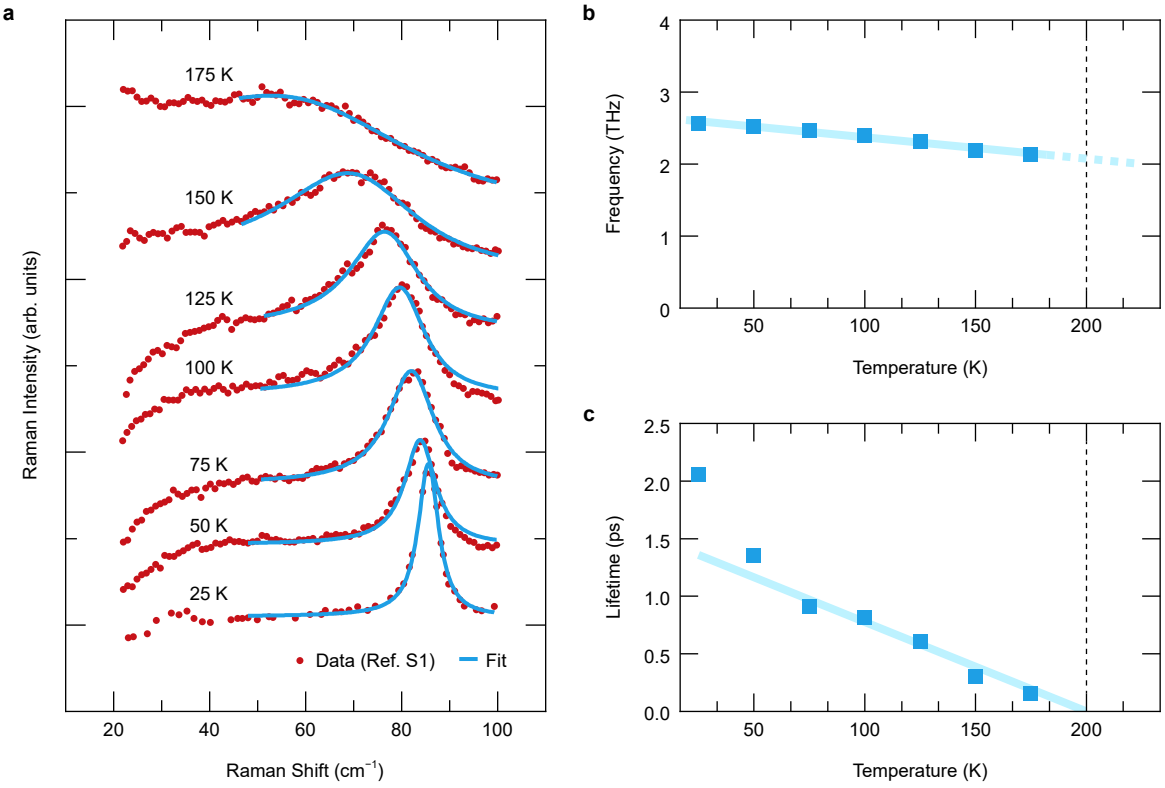

FIG. S2: **Analysis of Raman data.** **a**, Raman data taken from Fig. 2(b) of Ref. S3 with accompanying fits to a damped harmonic oscillator model, as discussed in the text. Curves are offset for clarity. **b**, Temperature dependence of the natural frequency $(\omega_0/2\pi)$ of the Raman mode extracted from the fits. The line is a guide to the eye. (c) Temperature dependence of the lifetime (τ) of the Raman mode extracted from the fits. The line is a guide to the eye.

S4. TIME-DEPENDENT LANDAU THEORY DETAILS

Numerical solutions. Here we take the full analytical expression of $\mathbf{D}_{11}(\omega)$ given by Eqns. (S6) and (S7) of Section S1 and solve numerically for different parameter values. Results are summarized in Fig. S3. The weak linear temperature dependence of the mode frequency observed by experiment is beyond the scope of our theory. We find instead a fairly constant mode frequency, with a slight upturn in the regime close to T_c. Indications of this upturn are not apparent in the data, likely because the mode lifetime becomes so short near T_c that it becomes difficult to extract meaningful phonon parameters from the experimental data in this regime. To construct Fig. S3, we use the fact that $\mathbf{D}_{11}(\omega)$ is a ratio of polynomials and is causal, and so it can be represented as a sum of poles in the lower half complex frequency plane. Finding the poles and their residues and Fourier transforming gives

$$\Phi(t) = B_0 + B_1 e^{-\gamma_1 t} + A_1 \sin(\Omega t) e^{-t/\tau}, \tag{S10}$$

where the term with coefficient B_1 is a pole on the imaginary axis representing overdamped dynamics of the Φ mode (which is induced by its coupling to the Ψ modes), and the term with coefficient A_1 represents the oscillations of the Φ mode, with the imaginary part of the pole giving the relaxation rate $1/\tau$ and the real part giving the frequency of oscillation Ω. One can in fact express the full solution for the poles analytically, but the equations are lengthy and we refrain from giving them here. Instead, we evaluate them numerically. If $\gamma_1 > 1/\tau$, the long-time dynamics are dominated by the third term of the above equation and the dynamics of the Φ mode are damped oscillations. If $\gamma_1 < 1/\tau$, the long-time dynamics are dominated by the monotonic behavior of the second term. We note that away from T_c we find $\gamma_1 > 1/\tau$, while the region close to T_c has $\gamma_1 < 1/\tau$. How well the crossover can be identified experimentally depends crucially on the prefactors B_1 and A_1 as well as the available temporal range of the data.

Next we consider the time domain, which is important because that is what is measured in experiment. Fig. S4 summarizes some numerical results for $\lambda = 0.9$, $\Omega_0/\gamma_0 = 0.6$, and $\Omega_0/2\pi = 2.5$ THz. One can clearly identify a dominant frequency up to a temperature $T \approx 185$ K, above which the monotonic relaxation becomes dominant and the subleading oscillatory behavior cannot be extracted reliably (we can still determine analytically where the poles sit and find that $\gamma_1 < 1/\tau$ at $T = 190$ K such that the oscillatory term be-

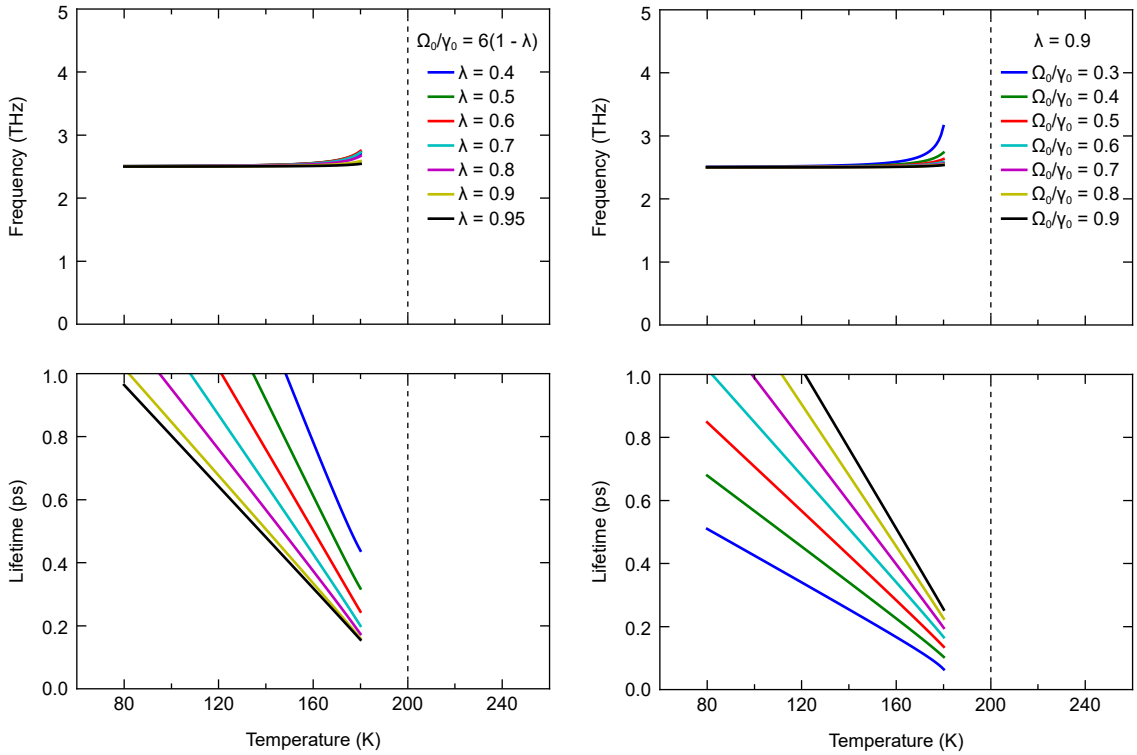

FIG. S3: **Summary of numerical results.** Frequency $\tilde{\omega} = \sqrt{\Omega^2 + 1/\tau^2}$ and lifetime τ for different values of γ_0 and λ. Other parameters are set to $\Omega_0/2\pi = 2.5$ THz, $T_c = 200$ K, and $\Omega_0/\gamma_0 = 6(1-\lambda)$ (left column) or $\lambda = 0.9$ (right column). For direct comparison, axes are scaled to match those in the main paper.

comes subdominant). The same can be concluded from the Fourier transform of the mode $\Phi(\omega) \sim D(\omega)$ at real frequency ω, which is shown in Fig. S5.

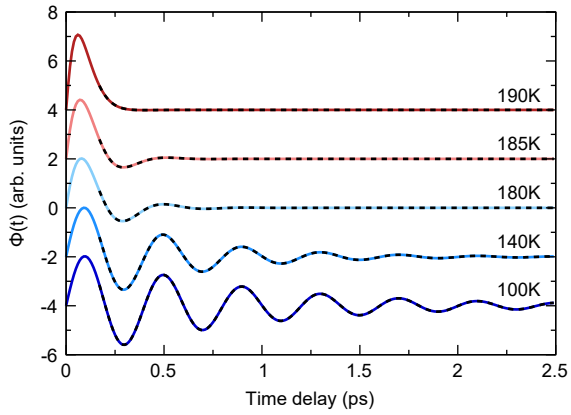

FIG. S4: **Time evolution of Φ.** Numerical simulation of the time dependence of $\Phi(t)$ (solid lines) for a selection of temperatures. The parameters used are $\lambda = 0.9$, $\Omega_0/\gamma_0 = 0.6$, and $\Omega_0/2\pi = 2.5$ THz. Dashed lines show fits to the data equivalent to those in the main text.

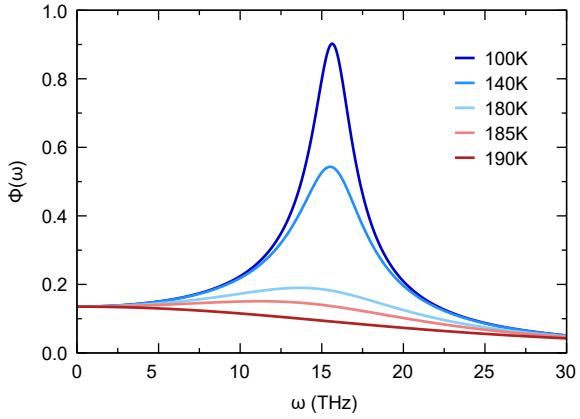

FIG. S5: **Frequency distribution of Φ.** The Fourier transform of $\Phi(t)$ for a selection of temperatures. The parameters used are $\lambda = 0.9$, $\Omega_0/\gamma_0 = 0.6$, and $\Omega_0/2\pi = 2.5$ THz.

Details of calculation. We begin with the free energy given in Eqn. (S1). By expanding around the equilibrium values given in Eqn. (S2) we find

$$\delta F = \frac{1}{2}\begin{pmatrix} \delta\Phi & \delta\Psi_u & \delta\Psi_g \end{pmatrix} \tilde{\mathbf{K}} \begin{pmatrix} \delta\Phi \\ \delta\Psi_u \\ \delta\Psi_g \end{pmatrix}, \tag{S11}$$

with force constant matrix $\tilde{\mathbf{K}}$ given by

$$\tilde{\mathbf{K}} = \begin{pmatrix} 1 & -\frac{\bar{g}}{\sqrt{2}}\bar{\Psi} & -\frac{\bar{g}}{\sqrt{2}}\bar{\Psi} \\ -\frac{\bar{g}}{\sqrt{2}}\bar{\Psi} & -t + \frac{3}{2}u\bar{\Psi}^2 & -\bar{g}\bar{\Phi} \\ -\frac{\bar{g}}{\sqrt{2}}\bar{\Psi} & -\bar{g}\bar{\Phi} & -t + \frac{3}{2}u\bar{\Psi}^2 \end{pmatrix}. \tag{S12}$$

If we assume overdamped dynamics (bare relaxation rate γ_0) for the Ψ modes, coherent dynamics for the Φ mode, and scale all frequencies to the bare oscillator frequency ω_0, we get the equation of motion

$$\begin{pmatrix} \frac{\omega^2}{\omega_0^2} & 0 & 0 \\ 0 & \frac{i\omega\gamma_0}{\omega_0^2} & 0 \\ 0 & 0 & \frac{i\omega\gamma_0}{\omega_0^2} \end{pmatrix} \begin{pmatrix} \delta\Phi \\ \delta\Psi_u \\ \delta\Psi_g \end{pmatrix} - \tilde{\mathbf{K}} \begin{pmatrix} \delta\Phi \\ \delta\Psi_u \\ \delta\Psi_g \end{pmatrix} = \text{Source}. \tag{S13}$$

The response to the probe that excites the "bare" Φ mode is the (1,1) component of

$$\tilde{\mathbf{D}}(\omega) = \left[\begin{pmatrix} \frac{\omega^2}{\omega_0^2} & 0 & 0 \\ 0 & \frac{i\omega\gamma_0}{\omega_0^2} & 0 \\ 0 & 0 & \frac{i\omega\gamma_0}{\omega_0^2} \end{pmatrix} - \tilde{\mathbf{K}} \right]^{-1}. \tag{S14}$$

This result is completely general. We can simplify in this particular case because Φ couples equally to Ψ_g and Ψ_u and the dynamical matrix for the Ψ fields is symmetric. Defining $\delta\Psi_\pm = \frac{1}{\sqrt{2}}\left(\delta\Psi_u \pm \delta\Psi_g\right)$, we have

$$\delta F = \frac{1}{2} \begin{pmatrix} \delta\Phi & \delta\Psi_+ & \delta\Psi_- \end{pmatrix} \mathbf{K} \begin{pmatrix} \delta\Phi \\ \delta\Psi_+ \\ \delta\Psi_- \end{pmatrix}, \tag{S15}$$

with

$$\mathbf{K} = \begin{pmatrix} 1 & -\bar{g}\bar{\Psi} & 0 \\ -\bar{g}\bar{\Psi} & -t + \frac{3}{2}u\bar{\Psi}^2 - \bar{g}\bar{\Phi} & 0 \\ 0 & 0 & -t + \frac{3}{2}u\bar{\Psi}^2 + \bar{g}\bar{\Phi} \end{pmatrix}, \tag{S16}$$

so the $\delta\Psi_-$ component decouples. The matrix that gives the response of the coupled $(\delta\Phi, \delta\Psi_+)$ modes is

$$\mathbf{D}(\omega) = \left[\begin{pmatrix} \frac{\omega^2}{\omega_0^2} - 1 & \bar{g}\bar{\Psi} \\ \bar{g}\bar{\Psi} & \frac{i\omega\gamma_0}{\omega_0^2} + t - \frac{3}{2}u\bar{\Psi}^2 + \bar{g}\bar{\Phi} \end{pmatrix} \right]^{-1}. \tag{S17}$$

In particular the experimentally measured $\delta\Phi$-$\delta\Phi$ response is given by the (1,1) component, which is

$$\mathbf{D}_{11}(\omega) = \frac{\frac{i\omega\gamma_0}{\omega_0^2} + t - \frac{3}{2}u\bar{\Psi}^2 + \bar{g}\bar{\Phi}}{\left(\frac{\omega^2}{\omega_0^2} - 1\right)\left(\frac{i\omega\gamma_0}{\omega_0^2} + t - \frac{3}{2}u\bar{\Psi}^2 + \bar{g}\bar{\Phi}\right) - \bar{g}^2\bar{\Psi}^2}. \tag{S18}$$

We identify the coefficient $\mathbf{D}_{11}(\omega)$, relating changes in the Φ field to the applied electric field (called "Source" in the calculation), as the conductivity, which is proportional to the measured change in the reflectivity. Let us rearrange this equation as

$$\mathbf{D}_{11}(\omega) = \frac{\omega_0^2}{\omega^2 - \omega_0^2\left(1 + \mathcal{S}(\omega)\right)}, \tag{S19}$$

with dimensionless mode self-energy

$$\mathcal{S}(\omega) = \frac{\bar{g}^2\bar{\Psi}^2}{\frac{i\omega\gamma_0}{\omega_0^2} + t - \frac{3}{2}u\bar{\Psi}^2 + \bar{g}\bar{\Phi}} = \lambda\frac{\frac{2t}{1-\lambda}}{\frac{i\omega\gamma_0}{\omega_0^2} - \frac{2t}{1-\lambda}}, \tag{S20}$$

where we have used the expressions for $\bar{\Psi}$ and $\bar{\Phi}$ in the second equality.

From the experimental data, we do not observe a large frequency shift as t is varied, implying that the real part of $\mathcal{S}$ depends only weakly on t for the relevant parameters. Thus, we must assume that $\frac{\omega\gamma_0}{\omega_0^2} \ll \frac{2t}{1-\lambda}$ so that the frequency shift remains negligible. This inequality must break down as $t \to 0$, but if $\gamma_0/\omega_0 \ll 1$ there is a wide range of t where it applies. In this limit, which is obtained for t sufficiently large ($T \ll T_c$), $\mathcal{S} \to -\lambda$. Defining the low-temperature renormalized (observable) mode frequency

$$\Omega_0 = \omega_0\sqrt{1-\lambda}, \tag{S21}$$

we have

$$\mathbf{D}_{11}(\omega) = \frac{\frac{\Omega_0^2}{1-\lambda}}{\omega^2 - \Omega_0^2 - \Pi(\omega)}, \tag{S22}$$

with

$$\Pi(\omega) = \Omega_0^2\frac{\lambda}{1-\lambda}\frac{-i\frac{\omega\Gamma}{\Omega_0^2} + \left(\frac{\omega\Gamma}{\Omega_0^2}\right)^2}{1 + \left(\frac{\omega\Gamma}{\Omega_0^2}\right)^2} \tag{S23}$$

and

$$\Gamma = \frac{(1-\lambda)^2}{2t}\gamma_0. \tag{S24}$$

Our theory therefore has only two fundamental degrees of freedom, λ and γ_0, and a range of λ and γ_0 describes the data. The range is constrained by the requirement that $\mathrm{Re}\left[\Pi(\omega)\right] \ll \Omega_0^2$. To construct Fig. 4 of the main text, we assumed $\gamma_0/2\pi = 3.5$ THz and adjusted λ as shown

in the figure. Our best fit of $\lambda = 0.85$ implies that the bare mode frequency $\omega_0/2\pi$ is $2.5/\sqrt{0.15}$ THz. Of course, other fits with slightly different γ_0 would also be possible.

[S1] J. He *et al., J. Electron. Mater.* **36**, 740-745 (2007).

[S2] J. W. Harter, L. Niu, A. J. Woss & D. Hsieh, *Opt. Lett.* **40**, 4671-4674 (2015).

[S3] C. A. Kendziora *et al., Phys. Rev. Lett.* **95**, 125503 (2005).

[S4] M. DiDomenico, Jr., S. H. Wemple, S. P. S. Porto & R. P. Bauman, *Phys. Rev.* **174**, 522-530 (1968).

[S5] G. Burns & B. A. Scott, *Phys. Rev. Lett.* **25**, 167-170 (1970).